Bulletin of the Seismological Society of America, Vol. 99, No. 2B, pp. 1404–1415, May 2009, doi: 10.1785/0120080067

Response Spectra for Near-Source, Differential, and Rotational Strong Ground Motion

by Reza S. Jalali and Mihailo D. Trifunac

Abstract It is shown that the pseudorelative spectral velocity (PSV) of an equivalent oscillator, which can be represented by a single degree-of-freedom system for excitation by synchronous horizontal excitation, can be extended to describe the PSV spectra of the same oscillator when excited by simultaneous action of horizontal, vertical, and rocking components of strong ground motion. At short periods, the new spectra are governed by differential ground motion and peak ground velocity, and they depend on the transit time of the waves along the length of the structure and on the oscillator frequency. At long periods, PSV spectral amplitudes tend toward an asymptote with amplitude proportional to the maximum rocking angle of ground motion.

Introduction

Since its introduction in the early 1930s (Trifunac, 2007), the response spectrum method (RSM) has become the principal vehicle for research and design work in earthquake engineering. The response spectra are used (1) to describe the amplitudes and frequency content of strong ground motion, (2) to serve as the starting point for the development of design codes (Freeman, 2007) and as scaling functions for frequency-dependent seismic zoning (Gupta, 2007), and (3) for selection of advanced design criteria of important structures. The first response spectra were defined for excitation by horizontal or vertical ground motions only, with other contributions to the relative response, which result from rocking and torsional components of strong ground motion (Gupta and Trifunac, 1989) having been considered only recently.

Analyses of two-dimensional models of long buildings show that when $a/\lambda < 10^{-4}$, where a is the wave amplitude of ground motion and λ is the corresponding wavelength, the wave-propagation effects on the response of simple structures can be neglected (Todorovska and Trifunac, 1990). For shorter waves—but those still longer than the characteristic dimensions of the structure—the common response spectrum method for synchronous ground motion can be extended to make it applicable for earthquake response analyses of extended structures experiencing differential in-plane and out-of-plane ground motion (Zembaty, 2007).

When engineering design is formulated via pushover analyses, the design is governed by target displacements determined from the inelastic response spectra of the corresponding single-degree-of-freedom (SDOF) system (Applied Technology Council [ATC], 1996; Federal Emergency Management Agency [FEMA], 1997, 2000; Aydinoglu, 2007). For estimation of the maximum nonlinear response of an SDOF system, u_m, in terms of the maximum linear response, u_0 (Fig. 1a), it is necessary to specify a relation between u_m and u_0. By defining the yield-strength-reduction factor as $R_y = u_0/u_y$, where u_y is the yielding displacement of the SDOF system-equivalent spring, and defining ductility as $\mu = u_m/u_y$, for the same ground motion the ratio u_m/u_0 is then equal to μ/R_y. Veletsos and Newmark (1960) showed that (1) for a long-period SDOF system, when its natural period T_n becomes very long, u_m/u_0 tends to 1 and R_y approaches μ (equal deformation rule); (2) for the response amplitudes governed mainly by the peak excitation velocities, u_m/u_0 can be approximated by $\mu/\sqrt{2\mu-1}$ and R_y by $\sqrt{2\mu-1}$ (equal strain energy rule); and (3) for a high-frequency (stiff) system when $T_n \sim 0$, $R_y \sim 1$. Departures from these rules have been described by Riddell and Newmark (1979) and were reviewed more recently by Jalali and Trifunac (2007, 2008). With reference to the more recent developments, we note that inelastic spectrum for constant target ductility is associated with the traditional strength-based design. The emerging deformation-based design via pushover analysis is associated with the inelastic displacement spectrum for specified yield-strength-reduction factor, which is obtained from the pushover analysis (Priestley *et al.*, 2007).

The first step in the engineering design of earthquake-resistant structures that use the RSM is the selection of the response spectrum shape and its amplitudes. In the beginning, this was accomplished by fitting, by hand, an envelope to a small number of the response spectra computed from several recorded accelerograms (Biot, 1934, 1941). Since the mid-1970s, following the systematic processing and archiving of recorded strong-motion accelerograms (Hudson, 1976), it became possible to develop empirical scaling equations, which directly give spectral amplitudes in terms of the

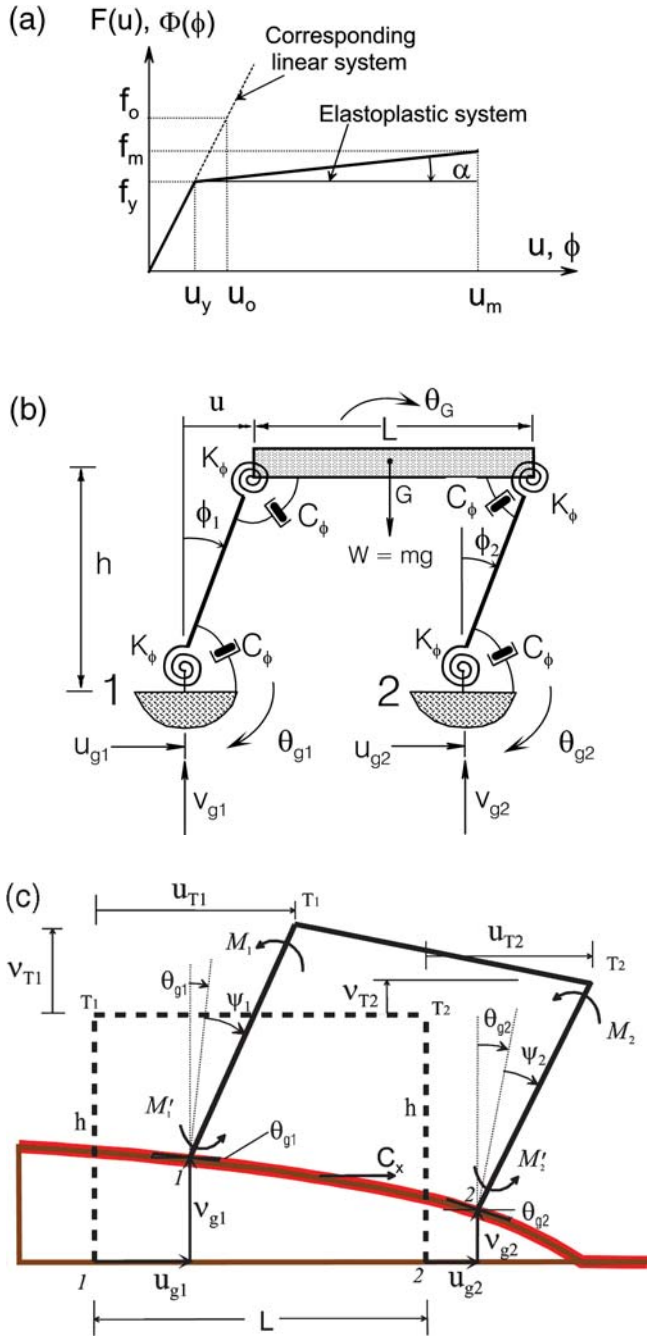

Figure 1. (a) Force-displacement (F, u) and moment-rotation (Φ, ϕ) relationships for bilinear spring. (b) Relative responses of the system excited by differential ground motions u_{g_1}, v_{g_1}, θ_{g_1}, u_{g_2}, v_{g_2}, θ_{g_2} at the base of its two columns 1 and 2. (c) The system deformed by the wave, propagating from left to right, with phase velocity C_x, for the case of $+v_{g_i}$ (up motion).

relevant scaling parameters (Lee, 2002, 2007; Douglas, 2003) or in terms of the given Fourier amplitude spectra (Udwadia and Trifunac, 1974). Because the recorded strong-motion data are relatively abundant only for fault-to-site distances in the range from several tens of kilometers to about 100 km, the empirical equations for scaling the spectral amplitudes are reliable and work well for the same distance range. Severe damage to structures, however, usually occurs in the near field of shallow earthquakes at distances that are less than 20–30 km. The strong ground motion near faults also includes near-field terms (Haskell, 1969) and strong-motion pulses, with large peak velocities and strong and sudden rotations (Trifunac, 2009) that change not only the spectral amplitudes but also their shape.

The purpose of this article is to describe how the spectral amplitudes for a simple representation of near-fault (at or close to the fault surface) motions differ from the familiar spectral shapes of motions at some distance (several tens of kilometers) from faults; we also describe how they depend on the differential motion of individual foundations and on large peak velocities and large rocking of ground motion for a simple structure subjected to these motions. Analyses of the consequences of other more complex aspects of near-fault motions, such as those caused by nonuniform soil properties, nonlinear transient and permanent soil deformations, soil-structure interaction, and lateral spreading, for example, are beyond the scope of this article.

Together with several previous studies of the effects of differential strong motion on the response of simple structures (Trifunac and Todorovska, 1997; Trifunac and Gičev, 2006) and of how the strength-reduction factors are affected by the proximity to the earthquake fault (Jalali and Trifunac, 2007, 2008; Jalali *et al.*, 2007), this article also aims to show how the classical response spectrum method can be extended to apply for physical conditions that are well beyond its original formulation. The role of simultaneous action of all six components of ground motion (three translations and three rotations; Trifunac and Todorovska, 2001) is still rarely considered in engineering design (Trifunac, 2006), even though it has been 75 years since the response spectrum method was formulated and about 40 years since it became the principal tool in engineering design (Trifunac, 2003). Because the response spectrum method has become an essential part of engineering design, we hope that the present work will help in providing further understanding and extension of its limits of applicability.

The Model

The nature of relative motion of individual column foundations or of the entire foundation-structure system will depend upon the type of foundation, the soil surrounding the foundation, the type of incident waves, and the direction of wave arrival so that at the base of each column the motion has six degrees of freedom. In this article, we consider only the in-plane horizontal, vertical, and rocking components of motion of column foundations and perform analysis for a simple model of a structure supported by just two isolated foundations. We assume that the structure is near the fault and that the longitudinal axis of the structure (x axis) coincides with the radial direction of the propagation of waves from the earthquake source so that the displacements at the base of the columns are different as a result of the wave pas-

sage. We suppose that the excitations at the piers have the same amplitude but different phases. The phase difference (or time delay) will depend only upon the distance between the piers and the horizontal phase velocity of the incident waves.

The model we employ in this article is described in Figure 1b,c. It represents a one-story structure consisting of a rigid mass, m, with length L, supported by two rigid massless columns with height h, which are connected at the top to the mass and at the bottom to the ground by rotational springs (Fig. 1b). The stiffness of the springs, k_ϕ, can in general be nonlinear (Jalali and Trifunac, 2007, 2008), as suggested in Figure 1a; however, in this article, we will consider the linear k_ϕ only. The massless columns are connected to the ground and to the rigid mass by rotational dashpots, c_ϕ, providing a fraction of critical damping equal to 5%. Rotation of the columns, ϕ_i, $i = 1, 2$, which is not assumed to be small, allows us to consider the geometric nonlinearity. The mass is acted upon by the acceleration of gravity, g, and is excited by differential horizontal, vertical, and rocking ground motions, u_{g_i}, v_{g_i}, and θ_{g_i}, $i = 1, 2$ (Fig. 1c) at two bases, so that

$$\begin{aligned} u_{g_2}(t) &= u_{g_1}(t-2\tau)\ ; \qquad v_{g_2}(t) = v_{g_1}(t-2\tau); \\ \theta_{g_2}(t) &= \theta_{g_1}(t-2\tau); \qquad \tau = L/(2C_x), \end{aligned} \tag{1}$$

where 2τ is the time delay between motions at the two piers and C_x is the horizontal phase velocity of incident waves. The functional forms of u_{g_i}, v_{g_i}, and θ_{g_i} are defined by near-source ground motions d_F and d_N, which are described in the next section. The governing differential equation for the system in Figure 1b,c is then (Jalali and Trifunac 2007)

$$\begin{aligned} &\left(A + \frac{(B\cos\phi_1 - C\sin\phi_1)}{(B\cos\phi_2 - C\sin\phi_2)}D\right)\ddot{\phi}_1(t) \\ &\qquad + \left(F - \frac{E}{(B\cos\phi_2 - C\sin\phi_2)}D\right) = 0, \\ &(L + u_{g_2} + h\sin\phi_2 - u_{g_1} - h\sin\phi_1)^2 \\ &\quad + [v_{g_2} - h(1-\cos\phi_2) - v_{g_1} + h(1-\cos\phi_1)]^2 - L^2 = 0, \end{aligned} \tag{2}$$

where

$$\theta_G = \sin^{-1}\left(\frac{v_{g_1} - v_{g_2} - h(1-\cos\phi_1) + h(1-\cos\phi_2)}{L}\right),$$

$$\dot{\theta}_G = \frac{\dot{v}_{g_1} - \dot{v}_{g_2} - h\sin\phi_1\dot{\phi}_1 + h\sin\phi_2\dot{\phi}_2}{L\cos\theta_G}, \tag{3a}$$

$$\begin{aligned} A = &-\frac{1}{2} + \left[-\frac{1}{4}\sin\phi_1\cos(\phi_1 - \theta_G) + \frac{\sin\phi_1\cos\phi_1}{12\cos\theta_G}\right] \\ &\times\left(\frac{\sin(\phi_2 - \phi_1)}{\cos\theta_G\cos\phi_1\cos\phi_2 + \frac{1}{2}\sin\theta_G\sin(\phi_1 + \phi_2)}\right), \end{aligned} \tag{3b}$$

$$\begin{aligned} B &= \frac{L + u_{g_2} - u_{g_1}}{h} + \sin\phi_2 - \sin\phi_1; \\ C &= \frac{v_{g_2} - v_{g_1}}{h} + \cos\phi_2 - \cos\phi_1, \end{aligned} \tag{3c}$$

$$\begin{aligned} D = &-\frac{1}{2}\cos(\phi_2 - \phi_1) \\ &+ \left[-\frac{1}{4}\sin\phi_2\cos(\phi_1 - \theta_G) - \frac{\sin\phi_2\cos\phi_1}{12\cos\theta_G}\right] \\ &\times\left(\frac{\sin(\phi_2 - \phi_1)}{\cos\theta_G\cos\phi_1\cos\phi_2 + \frac{1}{2}\sin\theta_G\sin(\phi_1 + \phi_2)}\right), \end{aligned} \tag{3d}$$

$$\begin{aligned} E = &\left(\frac{\dot{u}_{g_2} - \dot{u}_{g_1}}{h} - \cos\phi_1\dot{\phi}_1 + \cos\phi_2\dot{\phi}_2\right)^2 \\ &+ \left(\frac{\dot{v}_{g_2} - \dot{v}_{g_1}}{h} + \sin\phi_1\dot{\phi}_1 - \sin\phi_2\dot{\phi}_2\right)^2 \\ &+ B\left(\frac{\ddot{u}_{g_2} - \ddot{u}_{g_1}}{h} + \sin\phi_1\dot{\phi}_1^2 - \sin\phi_2\dot{\phi}_2^2\right) \\ &+ C\left(\frac{\ddot{v}_{g_2} - \ddot{v}_{g_1}}{h} + \cos\phi_1\dot{\phi}_1^2 - \cos\phi_2\dot{\phi}_2^2\right), \end{aligned} \tag{3e}$$

$$\begin{aligned} F = &-\frac{1}{2}\cos\phi_1\left(\frac{\ddot{u}_{g_2} + \ddot{u}_{g_1}}{h} - \sin\phi_1\dot{\phi}_1^2 - \sin\phi_2\dot{\phi}_2^2\right) \\ &+ \left[\frac{g}{h} + \frac{1}{2}\left(\frac{\ddot{v}_{g_2} + \ddot{v}_{g_1}}{h} - \cos\phi_1\dot{\phi}_1^2 - \cos\phi_2\dot{\phi}_2^2\right)\right]\left(\sin\phi_1\right. \\ &\left.+ \frac{1}{2}\frac{\cos(\phi_1 - \theta_G)\sin(\phi_2 - \phi_1)}{\cos\theta_G\cos\phi_1\cos\phi_2 + \frac{1}{2}\sin\theta_G\sin(\phi_1 + \phi_2)}\right) \\ &- \frac{1}{12}\frac{L\cos\phi_1}{h\cos\theta_G}\left[\frac{h}{L}\left(\frac{\ddot{v}_{g_1} - \ddot{v}_{g_2}}{h} - \cos\phi_1\dot{\phi}_1^2 + \cos\phi_2\dot{\phi}_2^2\right)\right. \\ &\left.+ \sin\theta_G\dot{\theta}_G^2\right] \\ &\times\left(\frac{\sin(\phi_2 - \phi_1)}{\cos\theta_G\cos\phi_1\cos\phi_2 + \frac{1}{2}\sin\theta_G\sin(\phi_1 + \phi_2)}\right) \\ &+ \left\{(M_1 + M_2)\cos\phi_1 + \frac{L}{2h}\sin\theta_G\left[(M_2 + M_2')\frac{\cos\phi_1}{\cos\phi_2}\right.\right. \\ &\left.\left.- (M_1 + M_1')\right]\right\} \\ &\times\left(\frac{h}{L}\frac{\sin(\phi_2 - \phi_1)}{\cos\theta_G\cos\phi_1\cos\phi_2 + \frac{1}{2}\sin\theta_G\sin(\phi_1 + \phi_2)}\right) \\ &- (M_2 + M_2')\frac{\cos\phi_1}{\cos\phi_2} - M_1 - M_1', \end{aligned} \tag{3f}$$

$$
\begin{aligned}
M_1 &= \frac{\omega_n^2}{4}\Phi(\phi_1 - \theta_G) + \frac{1}{2}\varsigma\omega_n(\dot{\phi}_1 - \dot{\theta}_G);\\
M_2 &= \frac{\omega_n^2}{4}\Phi(\phi_2 - \theta_G) + \frac{1}{2}\varsigma\omega_n(\dot{\phi}_2 - \dot{\theta}_G);\\
M_1' &= \frac{\omega_n^2}{4}\Phi(\phi_1 - \theta_{g_1}) + \frac{1}{2}\varsigma\omega_n(\dot{\phi}_1 - \dot{\theta}_{g_1});\\
M_2' &= \frac{\omega_n^2}{4}\Phi(\phi_2 - \theta_{g_2}) + \frac{1}{2}\varsigma\omega_n(\dot{\phi}_2 - \dot{\theta}_{g_2}).
\end{aligned}
\tag{3g}
$$

In equation (3), when $\tau = 0$, ω_n and ς become the circular natural frequency and damping ratio of the equivalent SDOF system; $\Phi(\phi)$ is, in general, a nonlinear function of the type described in Figure 1a. For $\tau \neq 0$, the rigid mass with length L behaves as a three-degrees-of-freedom (3DOF) system experiencing horizontal and vertical translations of G and rotation θ_G (see Fig. 1b,c). Through relative rotations between the mass and the two columns, which give rise to different axial forces and moments in two columns, the two inertial forces from two translations, and the inertial moment associated with $\ddot{\theta}_G$, the rigid mass behaves like a 3DOF system. Because of the assumed continuity of soil between the two foundations, along with *a priori* specified motion at the two supports (we are assuming that there is no soil-foundation-column interaction at two foundations), geometrical constraints enable a description of this dynamic problem in terms of only one function of time [$\phi_1(t)$ or $\phi_2(t)$].

Near-Source Ground Motion

We cannot predict the details of the near-fault (close to and on the fault surface) ground motion due to unknown and irregular distribution of fault slip and geologic rigidities surrounding the fault, nonuniform distribution of stress and of stress drop on the fault, and complex nonlinear processes that accompany the faulting (e.g., Takeo and Ito, 1997). In the current article, we adopt a simplified approach and illustrate these motions by working with their substitutes that have carefully chosen amplitudes and durations and that have been compared with and calibrated against the observed fault slip and the recorded strong motions in terms of their peak amplitudes in time and their spectral contents (Trifunac, 1993a, 2009).

Figure 2 schematically shows a plan view of the vertical strike-slip fault and two motions, d_N and d_F, which illustrate fault-parallel displacement and a fault-normal pulse. We represent the fault-normal pulse with (Fig. 2, center)

$$d_F(t) = A_F t e^{-\alpha_F t}, \tag{4}$$

where the typical values of A_F and α_F for different earthquake magnitudes are shown in Table 1 (Trifunac, 2009). Because the recorded strong-motion data are abundant only up to about M 6.5, the values of α_F and A_F, for M 7 and 8, in Tables 1 and 2, are enclosed by parentheses to emphasize that these are based on extrapolation. We represent the near-fault-parallel displacement with (Fig. 2, bottom)

$$d_N(t) = \frac{A_N}{2}(1 - e^{-t/\tau_N}). \tag{5}$$

The values of A_N and τ_N are given in Table 2.

The amplitudes analogous to d_F and d_N have been studied in many regression analyses of recorded peak displacements at various distances from the fault and in terms of the observed surface expressions of fault slip. In seismological papers, the d_N amplitudes are traditionally presented in terms

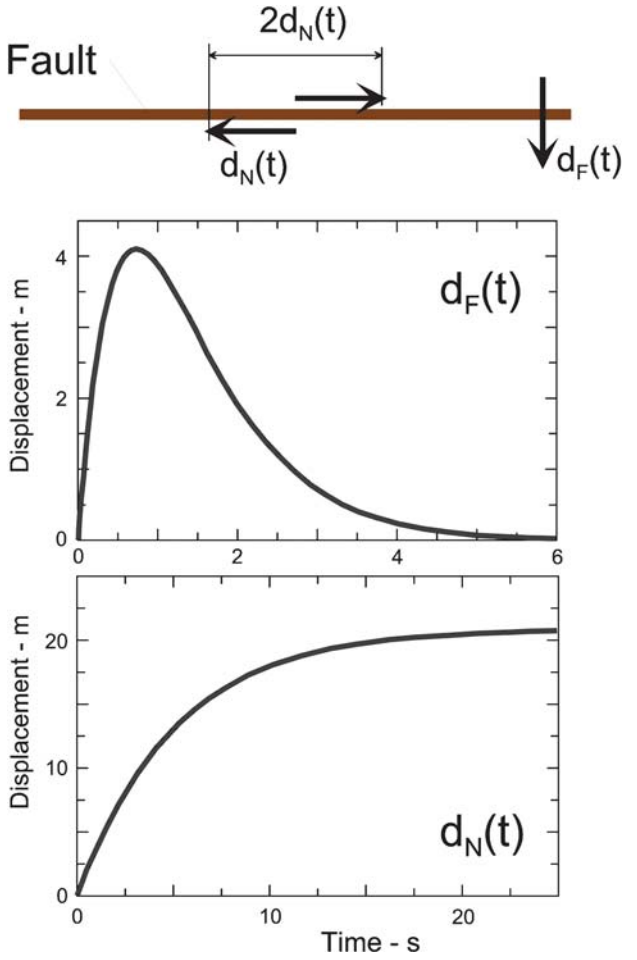

Figure 2. Fault-parallel, $d_N(t)$, and fault-normal (pulse), $d_F(t)$, displacements adopted to represent near-fault motions in this study.

Table 1
Characteristics of Fault-Normal Pulse Displacement

M	α_F (1/sec)	A_F (cm/sec)	$d_{F,\max}$ (cm)	$\dot{d}_{F,\max}$ (cm/sec)
4	14.04	56.48	1.5	56.5
5	7.90	151.61	7.1	152.
6	4.44	546.97	45.3	547.
7	(2.50)	(860.34)	(127.)	(860.)
8	(1.40)	(1560.29)	(410.)	(1560.)

Table 2
Characteristics of Fault-Parallel Displacement

M	τ_N (sec)	A_N (cm)	$d_{N,\max}$ (cm)	$\dot{d}_{N,\max}$ (cm/sec)
4	0.55	4.9	2.5	4.5
5	1.2	29.2	14.6	12.2
6	1.8	245.5	123.	68.2
7	(3.0)	(1288.0)	(644.)	(215.)
8	(5.0)	(4169.0)	(2084.)	(417.)

of average dislocation amplitudes, $\bar{u}$, which are related to d_N, as $\bar{u} = 2d_N$ (Fig. 2, top). Average dislocation is the value of dislocation amplitudes averaged over the fault surface and is the quantity used in spectral interpretations of near-field (extending to about one source dimension from the fault) motions and of the body-wave amplitudes in the far field (beyond about ten source dimensions).

An important property of the d_F and d_N for this article lies in their initial velocity, $\dot{d}_F \sim \sigma\beta/\mu$, where σ is the effective stress (~stress drop) on the fault surface, β is the velocity of shear waves in the fault zone, and μ is the rigidity of rocks surrounding the fault. For $\dot{d}_N$ it can be shown that $\dot{d}_N = 0.5C_0\sigma\beta/\mu$ at $t = 0$, where typical values of C_0 are 0.6, 0.65, 1.00, 1.52, and 1.52 for M 4, 5, 6, 7, and 8, respectively (Trifunac, 1998, 2009).

Amplitudes of the pseudorelative spectral velocity (PSV) of the linear response of SDOF systems can be viewed and scaled in three period ranges, where the PSV amplitudes are dominated by (1) peak ground acceleration, (2) peak ground velocity, and (3) peak ground displacement (Veletsos *et al.*, 1965). The boundaries between these three period ranges depend on the size of the earthquake, the epicentral distance (via frequency-dependent attenuation), and local site conditions. The velocity period range, for example, is centered near the peak spectral amplitudes and moves from near 1 Hz for $M \sim 8$ to 6 Hz for $M \sim 4$ (Trifunac, 1993b, 1994). When the fault motions d_F and d_N begin with a sudden jump in ground velocity (caused by a sudden stress drop on the fault surface), this large initial velocity will dominate the spectral amplitudes; for the short periods of the oscillator, the acceleration-dominated zone of PSV amplitudes will disappear. This will result in essentially constant PSV amplitudes in the short-period range (wide gray lines in Fig. 3a,b).

An example of the ground-displacement pulse perpendicular to the fault—which was recorded at station 2 of the five-station array at Sholame during the Parkfield, California, earthquake of 1966 (Housner and Trifunac, 1967) about 3 km above and about 10 km southeast from the principal fault slip (Trifunac and Udwadia, 1974)—is a near-field (not near-fault) pulselike ground motion that may have left

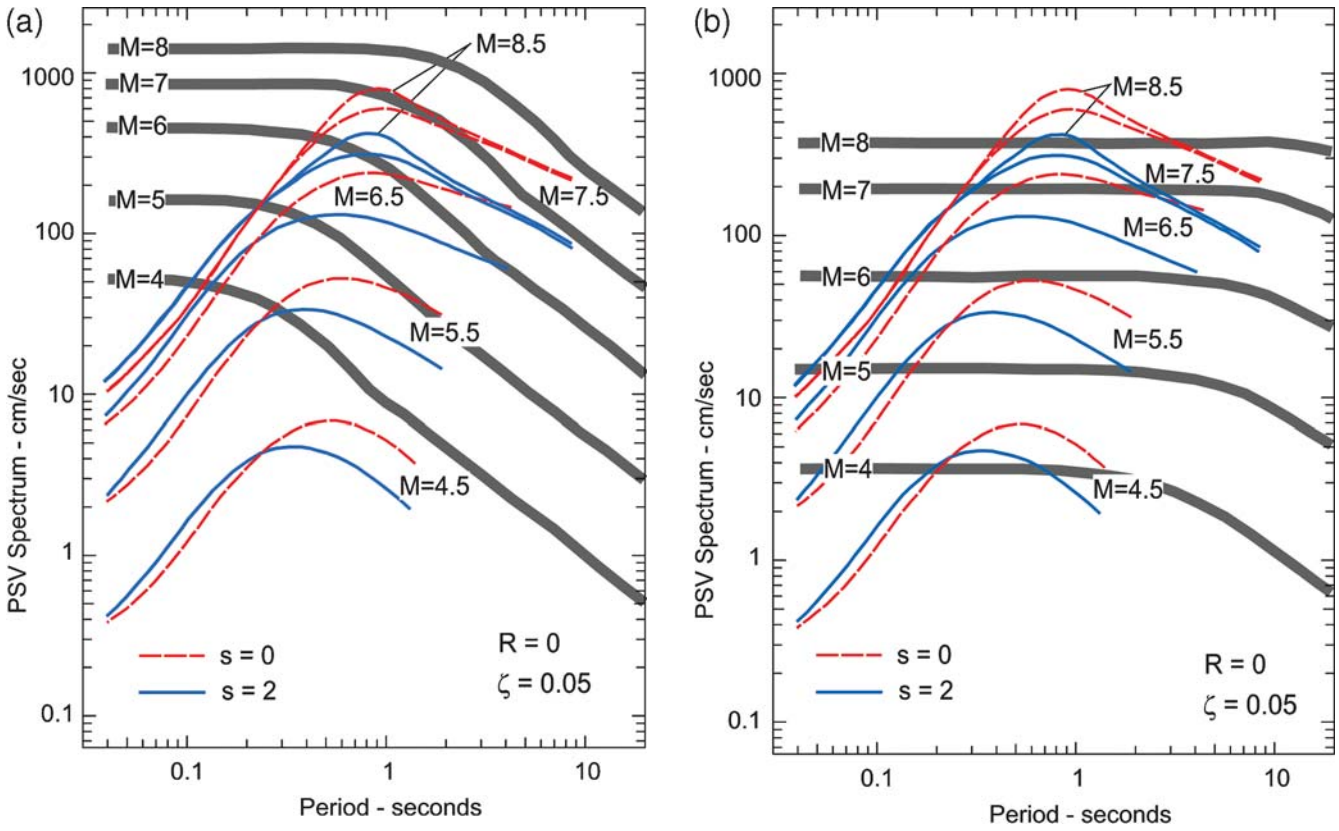

Figure 3. Comparison of PSV spectra for (a) d_F, fault-normal pulse (wide gray lines) and for (b) d_N, fault-parallel displacement (wide gray lines), with average PSV spectra at fault, based upon regression analysis of recorded strong ground motion (Trifunac, 1978), for sites on sediments ($s = 0$) and on basement rock ($s = 2$).

the fault surface as d_F but was subsequently attenuated and filtered along its 11 km path between the southeastern end of the fault slip and the recording station. The ground displacement recorded at the Pacoima Dam, several kilometers above the fault, during the San Fernando, California, earthquake of 1971 (Trifunac, 1974) can serve as an illustration of a fault-parallel motion, d_N, recorded above a thrust fault (but not on the fault). These two examples lend support to our choice of the simple fault displacement functions d_F and d_N. The functions d_F and d_N model the displacement time histories in the fault-normal and fault-parallel directions. For vertical strike-slip faults, d_F and d_N will also represent strike-normal and strike-parallel motions along the surface expression of the fault. For dip-slip faults, a linear combination of d_F and d_N will contribute only to the vertical and strike-normal displacements on the ground surface. For a general fault orientation, both d_F and d_N will contribute to the surface displacements, as determined by their projections onto horizontal and vertical motions on the ground surface (Mavroeidis and Papageorgiou, 2003). In the following, we will refer to d_F and d_N in the context of vertical strike-slip faults only.

For simplicity, in this article we assume that the vertical ground motion $v_{g_i}(t) = \pm u_{g_i}(t)$ and the functional form of $u_{g_i}(t)$ is defined by equations (4) and (5) for the fault-normal pulse and fault-parallel displacement, respectively. In the following, we will refer to the results for $+v_{g_i}$ as up and to those for $-v_{g_i}$ as down. The rocking component of the ground motion will be approximated by (Trifunac, 1982; Lee and Trifunac, 1987)

$$\theta_{g_i}(t) = \left(-\frac{1}{C_x}\right)\dot{v}_{g_i}(t), \tag{6}$$

where $\dot{v}_{g_i}(t)$ is the vertical velocity of the ground motion. Of course, in modeling with more detail, the ratio of v_{g_i} to u_{g_i} amplitudes will depend upon the incident angle and the character of incident waves, while the associated rocking θ_{g_i} will be described by a superposition of rocking angles associated with incident body and dispersed surface waves (Trifunac, 1971; Wong and Trifunac, 1979).

To emphasize how different the PSV spectral amplitudes and shapes are for d_F and d_N excitations, we superimpose the average PSV spectra estimated by regression analysis of PSV spectral amplitudes computed from recorded accelerograms in the western United States in Figure 3a,b. Those are for motions on sediments ($s = 0$) or on geological basement rock ($s = 2$) for a fraction of critical damping $\varsigma = 0.05$ at epicentral distance $R = 0$ km and for magnitudes M 4.5, 5.5, 6.5, 7.5, and 8.5 (Trifunac, 1978).

PSV Spectra for Near-Fault Strong Ground Motions

In the following, we describe the PSV of linear response to ground motions d_F and d_N. To avoid clutter, we present the spectral curves for M 4, 6, and 8 only for 5% critical damping and for periods 0.05–20 sec. To show the relative significance of two translations and one rotation (rocking), we compare spectra for (1) horizontal motion only (u_g), (2) simultaneous action of horizontal and vertical motions (u_g and v_g), and (3) simultaneous action of horizontal and vertical translations and of rocking (u_g, v_g, and θ_g). We illustrate the spectral amplitudes of in-plane response only. Analysis of the response spectra for coupled in- and out-of-plane excitation and response, along with analysis for nonlinear (material) response, is beyond the scope of this article.

For the model shown in Figure 1b,c, we define the PSV spectrum amplitudes at the top and at the bottom corners of the model as follows:

$$\text{at } i\text{ th top corner:} \qquad \text{PSV}_i = \omega_n SD_i = \omega_n h \sin(\phi_i - \theta_G) \tag{7a}$$

$$\text{and at } i\text{ th bottom corner:} \quad \text{PSV}_i = \omega_n SD_i = \omega_n h \sin(\phi_i - \theta_{g_i}), \tag{7b}$$

where ϕ_i is the rotation of the ith column, computed from the solution of differential equations of the system response (equations 2 and 3). θ_{g_i} is the ground rocking at the base of the ith column, and θ_G is the rotation of the beam

$$\theta_G = \sin^{-1}\{[v_{g_1} - v_{g_2} - h(1 - \cos\phi_1) + h(1 - \cos\phi_2)]/L\}. \tag{8}$$

It can be seen that the rotation of the beam, θ_G, directly depends upon the differential vertical ground motion ($v_{g_1} - v_{g_2}$) and on the length of the model L. The PSV spectrum amplitudes at the top and bottom corners depend upon θ_G and θ_{g_i}, respectively.

The spectral amplitudes in Figure 4a,b were calculated for the fault-normal pulse d_F and for fault-parallel displacement d_N, respectively, with their amplitudes as shown in Tables 1 and 2. In all calculations, we employed nonlinear geometric characteristics of the system, as shown in equations (3) and (4); however, we assumed that the helical springs at the four corners, k_ϕ, remain linear. We chose the parameters of the system shown in Figure 1b,c so that it represents an equivalent single-degree-of-freedom oscillator representing the fundamental mode of an N-degree-of-freedom building with N stories. Specifically, we selected the equivalent period of the oscillator to be $T = 0.1 \times N$ (seconds) and $h = 3.5 \times N \times 0.64$ (meters), where 3.5 is the height of an average story in meters and the factor 0.64 is the equivalent height factor for the sinusoidal mode shape (Trifunac and Todorovska, 1997). All of the calculations were carried out for a structure with $L = 20$ m.

In Figure 4a,b, we illustrate all spectra for vertical ground motion up (Fig. 1c). The spectra for vertical ground motion down show some differences, but for all periods they fluctuate about the shown spectra for up motions with only minor differences. For brevity's sake, we show only the spectra for vertical motions up.

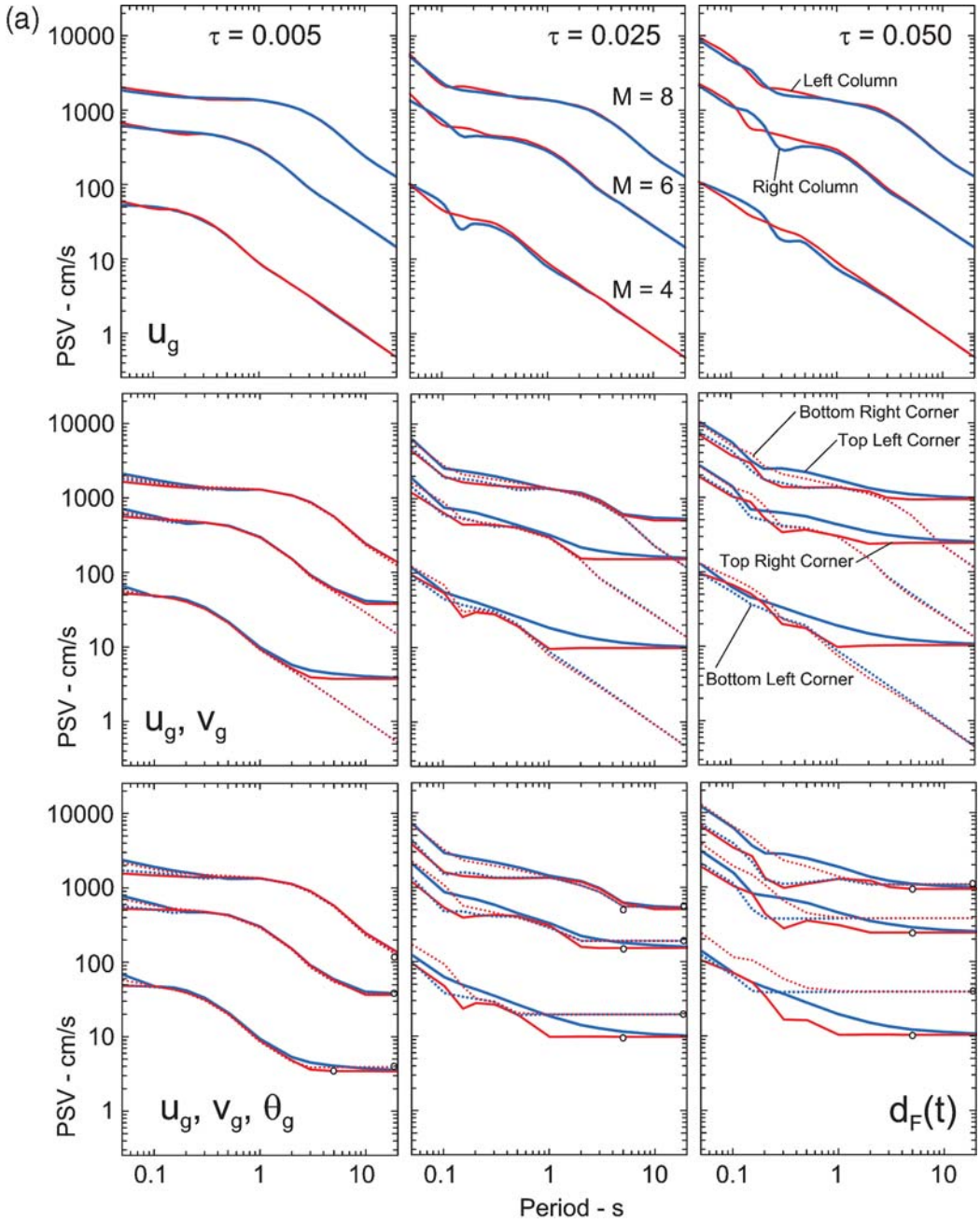

Figure 4. Matrix-type comparison for PSV spectra, for excitation by (a) d_F pulse and by (b) d_N, fault-parallel motion, for three wave transit times, from left to right foundation, equal to $2\tau = 0.01$, 0.05, and 0.10 (in three columns of the matrix, left to right), for three magnitudes M 4, 6, and 8, and for three excitations (1) by horizontal ground motion only (u_g), (2) by horizontal and vertical translations (u_g and v_g), and (3) with two translations (u_g and v_g) and one in-plane rocking (θ_g). Spectral amplitudes at the top corners of the model (where the columns meet the rigid mass) are shown with solid lines; the spectra at the bottom corners (where the columns are connected to the ground) are shown with dashed lines. (*Continued*)

PSV Spectra at Long Periods

For soft k_ϕ (long natural periods T), the rotation of the two columns (ϕ_1 and ϕ_2) becomes nearly the same for all three excitations considered in this article: (1) u_g, (2) $u_g + v_g$, and (3) $u_g + v_g + \theta_g$; it is very small, thus the effects of the vertical and rocking components of the ground motion on the response (ϕ_1 and ϕ_2) also become relatively small. For excitation by horizontal differential ground motion (u_g), the rocking of the beam is small relative to ϕ_1 and ϕ_2, so the relative rotation of the columns at the top and bottom becomes almost the same (top rows in Fig. 4a,b). For excitation by simultaneous horizontal and vertical ground motion $u_g + v_g$, because of the axial rigidity of the two columns and the differential vertical ground motion at the two piers ($v_{g_1} - v_{g_2}$), the rotation of the beam (θ_G) becomes large relative to ϕ_1 and ϕ_2 (center rows in Fig. 4a,b),

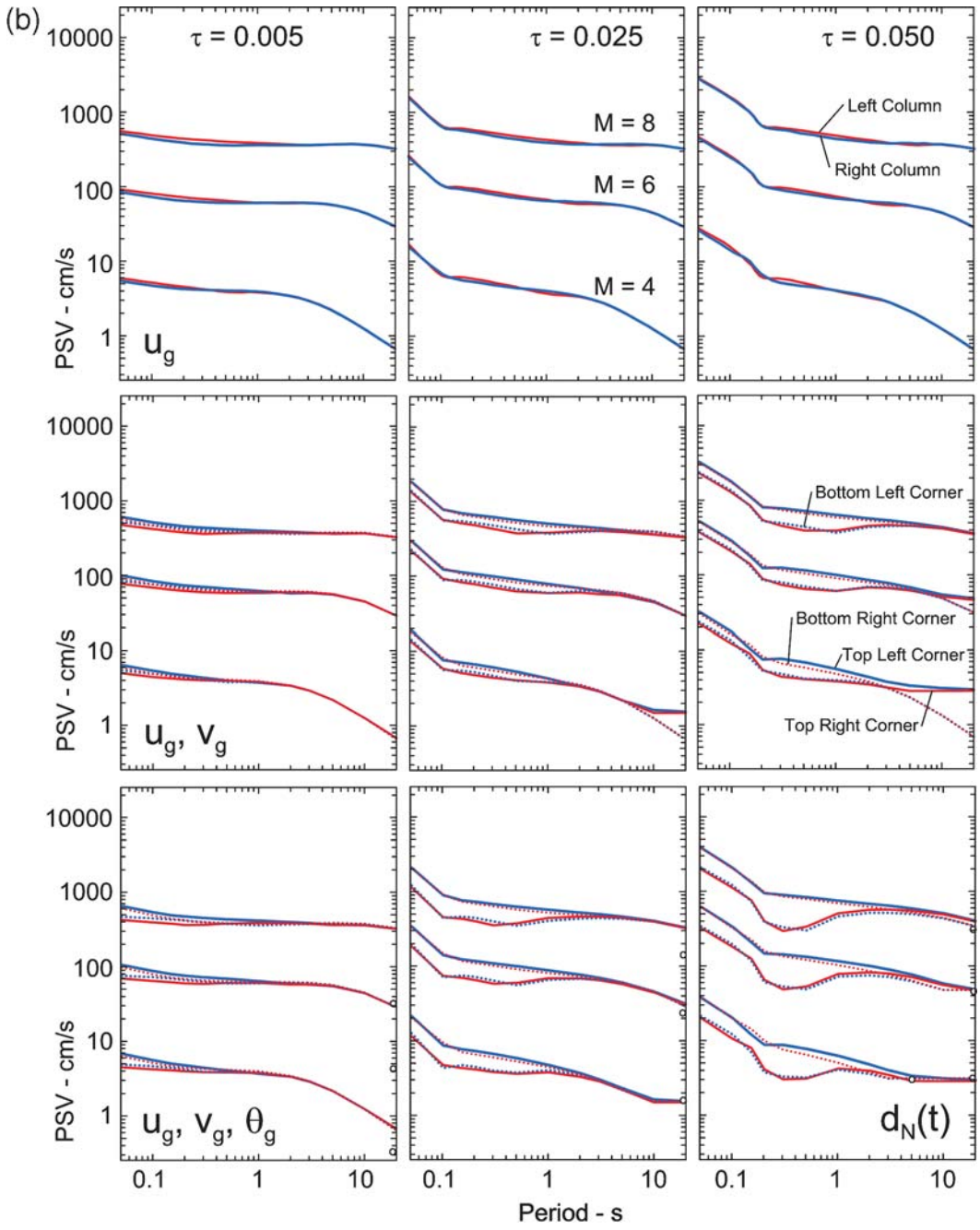

Figure 4. Continued.

so that the relative rotation of the columns at the top becomes larger than at the bottom. That is, at the bottom the relative rotation of columns does not change relative to the case (1) with u_g, corresponding to the horizontal excitation only (top rows in Fig. 4a,b). For simultaneous excitation by horizontal, vertical, and rocking ground motion, (3) $u_g + v_g + \theta_g$, the rocking of the beam, θ_G, and the rotation of the two columns, ϕ_1 and ϕ_2, do not change significantly relative to cases (1) and (2); however, because of the ground rocking (θ_{g_i}), the relative rotation of both columns at the bottom changes (bottom row in Fig. 4a,b). The aforementioned trends are essentially the same for both upward and downward excitation by v_g.

The results show that for nearly synchronous ground motion (small τ), the effect of the vertical and rocking components on the linear response of a long-period system is small (for zero time delay, the phase velocity is infinite; therefore, the rocking component of the ground motion at the two piers is equal to zero). The differential vertical ground motion mostly affects the relative rotation at the top corners; the rocking component of the ground motion mostly affects the relative rotation of columns at the bottom corners. These

trends are a direct consequence of the assumptions made in our model, wherein we assume that the beam and the columns are rigid and that the columns have separate and independent foundations. Consequently, the differential vertical ground motion at the two foundations is transferred directly to the top; for a long-period system, this results in the rotation of the top beam.

The consequences of the described trends are that for long periods, the PSV amplitudes as defined by equations (7a) and (7b) tend toward constant asymptotes

$$\mathrm{PSV}_{T\to\infty} = \omega_n h \sin\theta_{g,\max} \tag{9}$$

at the base of the columns and toward

$$\mathrm{PSV}_{T\to\infty} = \omega_n h \sin\theta_{G,\max} \tag{10}$$

at the top of the columns. In equation (9), $\theta_{g,\max}$ is the peak of the rocking angle of ground motion; in equation (10), when $T \to \infty$, $\theta_G \to (v_{g_1} - v_{g_2})/L$. Selected examples based directly on these asymptotic values are shown in Figure 4a,b by open circles at $T \sim 20$ sec for $\theta_{g,\max}$ at the bottom of columns and at $T = 5$ sec for $\theta_{G,\max}$ at the top of the columns. The asymptotic values in equation (9) are essentially reached for $T \sim 20$ sec and $\theta_{g,\max}$ in all examples shown in Figure 4a,b, except for $\tau = 0.005$ and 0.025 in Figure 4b. The asymptotic amplitudes based on equation (10) are shown in Figure 4a at $T = 5$ sec only for M 4 and $\tau = 0.050$ and in Figure 4a for all M except for M 6 and 8 and $\tau = 0.005$ because the spectra reach those asymptotes beyond $T \sim 20$ sec. It is seen that these asymptotic amplitudes are in excellent agreement with the calculated PSV amplitudes using equations (2) and (3).

PSV Spectra at Short Periods

It has been shown (Trifunac and Todorovska, 1997) that the relative displacement spectra at short periods (stiff structures) for in-plane differential horizontal ground motion (predominantly *P*, *SV*, and Rayleigh waves propagating along the longitudinal axis of the structure) become constant and equal to $\dot{u}_{g,\max}\tau$, where $\dot{u}_{g,\max}$ is the peak velocity of in-plane horizontal ground motion and τ is the travel time of the strong-motion waves from the extreme column to the center of the plane of the building [$\tau = L/(2C_x)$]. For out-of-plane excitation (predominantly *SH* and Love waves propagating along the longitudinal axis of a structure) and the resulting out-of-plane response (assuming that there is no coupling with in-plane excitation and in-plane response), it was shown that the relative displacement spectral amplitudes become $\sim 2\dot{u}_{g,\max}\tau$, where $\dot{u}_{g,\max}$ is the peak velocity of out-of-plane horizontal ground motion (Trifunac and Gičev, 2006). To calculate the PSV spectral amplitudes, we multiply the aforementioned values by ω_n.

The aforesaid estimates of the effects of differential ground motion on the high-frequency relative displacement spectrum amplitudes are based on the Taylor series approximation of ground strains and work well for excitation by long waves. When this assumption does not hold—that is, for excitation by short waves—the point derivative $\dot{u}_{g,\max}$ becomes an upper bound estimate and should be replaced by

$$\dot{\bar{u}}_{g,\max} = [u_{g2}(t + L/C_x) - u_{g1}(t)]/(L/C_x), \tag{11}$$

where $\dot{\bar{u}}_{g,\max}$ is the largest value of $\dot{\bar{u}}_g$ during excitation. Consequently, at short periods, the PSV amplitudes for the fault-normal pulse d_F and for fault-parallel displacement d_N will be dominated by

$$\mathrm{PSV}_{T\to\infty} = \omega_n \dot{\bar{u}}_{g,\max}\tau \tag{12}$$

for in-plane excitation, and by

$$\mathrm{PSV}_{T\to\infty} = \omega_n 2\dot{\bar{u}}_{g,\max}\tau \tag{13}$$

for out-of-plane excitation.

For our example, with displacements d_F and d_N (see equations 4 and 5), the reduction factors are equal to $\dot{\bar{u}}_{g,\max}/\dot{u}_{g,\max} = \exp(-\alpha_F 2\tau)$ and $\dot{\bar{u}}_{g,\max}/\dot{u}_{g,\max} = (\tau_N/2\tau)[1 - \exp(-2\tau/\tau_N)]$, respectively. For M 8, these reduction factors are 0.86 and 0.99, for the time delay $2\tau = L/C_x = 0.1$. For M 4, the corresponding reduction factors are 0.25 and 0.91, respectively. The example illustrated in Figure 5 shows how well the asymptotes in equation (12) describe the PSV amplitudes for excitation by u_g only and for $\tau = 0.025$ and 0.050 as $T \to 0$. For irregular and more complex ground motion, relative to our examples of d_F and d_N, it is more conservative to work with the upper bounds based on $\dot{u}_{g,\max}$—that is, to use

$$\mathrm{PSV}_{T\to\infty} = \omega_n \dot{u}_{g,\max}\tau \tag{14}$$

for in-plane excitation and

$$\mathrm{PSV}_{T\to\infty} = \omega_n 2\dot{u}_{g,\max}\tau \tag{15}$$

for out-of-plane excitation.

In this article, at short periods the relative displacement of the system tends toward zero, while the relative velocity is not zero but rather equal to the initial velocity of the ground, $\dot{u}_g(t = 0)$. Thus, there are two velocities contributing to the spectral amplitudes at short periods: initial velocity for synchronous motion, $\dot{u}_g(t = 0)$, and the velocity for differential motion of the system, $\omega_n \dot{u}_{g,\max}\tau$. The maximum velocity of the system, subjected to horizontal differential ground motion at short periods, is $\mathrm{PSV}_{T\to\infty} = [\dot{u}_g^2(t = 0) + (\omega \dot{u}_{g,\max}\tau)^2]^{1/2}$ by the square root of the sum of squares (SRSS) rule, where the first term is due to the synchronous horizontal ground motion and the second term is due to the horizontal differential ground motion. As can be seen from Figure 5, when $\tau \to 0$ (e.g., $\tau = 0.005$), the PSV amplitude tends to the asymptote $\dot{u}_g(t = 0)$, the initial velocity of the ground. For out-of-plane excitation, we would have $\mathrm{PSV}_{T\to\infty} = [\dot{u}_g^2(t = 0) + (2\omega \dot{u}_{g,\max}\tau)^2]^{1/2}$.

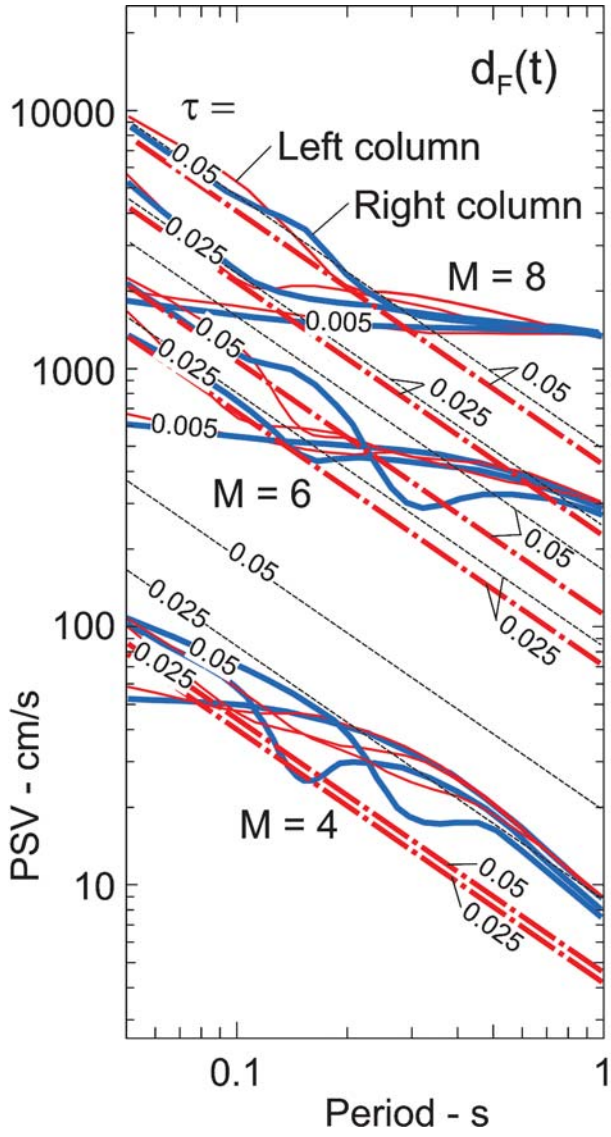

Figure 5. An example of how the computed PSV spectra (continuous light lines for left column and heavy continuous lines for right column) for excitation with a d_F pulse, along with M 4, 6, and 8, approach the asymptotes $\mathrm{PSV}_{T\to 0} = \omega_n \dot{u}_{g,\max}\tau$ for $\tau = 0.025$ and 0.05. Upper bounds in terms of $\omega_n \dot{u}_{g,\max}\tau$ are shown with light dotted lines; the asymptotes in terms of $\mathrm{PSV}_{T\to 0} = \omega_n \ddot{u}_{g,\max}\tau$ are shown with dash-dotted-dash lines.

Complete PSV Spectra for All Periods

A simple approximation, which combines the effects of all of the motions contributing to the PSV spectral amplitudes, is to use the SRSS combination rule (Goodman *et al.*, 1958) as follows

$$\mathrm{PSV}_{\mathrm{base}} = [\mathrm{PSV}^2(\tau = 0, \theta_g = 0) + (f\omega_n \dot{u}_{g,\max}\tau)^2 + (\omega_n h \sin\theta_{g,\max})^2]^{1/2} \quad (16)$$

at the base of the columns and

$$\mathrm{PSV}_{\mathrm{top}} = [\mathrm{PSV}^2(\tau = 0, \theta_g = 0) + (f\omega_n \dot{u}_{g,\max}\tau)^2 + (\omega_n h \sin\theta_{G,\max})^2]^{1/2} \quad (17)$$

at the top of the columns, where $\mathrm{PSV}(\tau = 0, \theta_g = 0)$ is the PSV for a given horizontal ground motion, which has peak ground velocity $\dot{u}_{g,\max}$. The peak rocking angle accompanying this motion can be approximated as in equation (6). Equation (17) can be used only if $\theta_G \to (v_{g_1} - v_{g_2})/L$ can be estimated from some other knowledge of vertical motions at the column supports v_{g_1} and v_{g_2}. A conservative approximation is to assume that $\mathrm{PSV}_{\mathrm{top}} \sim \mathrm{PSV}_{\mathrm{base}}$. Perusal of Figure 4a,b shows that for large motions, this is a fair approximation and that $\mathrm{PSV}_{\mathrm{top}}$ becomes significantly smaller than $\mathrm{PSV}_{\mathrm{base}}$ only for short pulses, which in our examples corresponds to M 4.

The emphasis in this article has been on the analysis of in-plane response in the case when the seismic waves propagate essentially along the longitudinal axis of the structure. For this case, in equations (16) and (17), $f = 1$. In the simplest case, the corresponding out-of-plane excitation consists of *SH* and Love waves only; hence it should have ground rocking in and about the propagation direction equal to zero, with $\theta_{g,\max} \sim 0$. However, real earth materials are inhomogeneous and do not consist of parallel layers of constant thickness; long structures are not oriented along the radial direction of the waves propagating from the earthquake source. Consequently, the mixing of different wave types and the three-dimensional scattering will result in $\theta_{g,\max}$, which may not be small. Therefore, to approximate the response spectra for out-of-plane response, which now also must include torsional excitation of the rigid mass, we take $f = 2$ (Trifunac and Gičev, 2006). This approximation is valid only for excitation by waves with wavelengths much longer than L and for cases in which the geometry of the structure does not lead to strong coupling of the in-plane and out-of-plane responses. Analysis of the out-of-plane response for intermediate and short waves, with wavelengths comparable to L, will be addressed in our future work.

Conclusions

We have shown that the PSV spectral amplitudes of linear response for excitation by horizontal, vertical, and rocking strong ground motion can be represented by superposition of three terms. The first term is the classical PSV spectrum for horizontal excitation only (u_g). For motions at some distance from the fault, when initial velocity in the response calculations can be assumed to be small, this term can be estimated via empirical scaling equations based on the recorded strong-motion data (Lee, 2002, 2007; Douglas, 2003). The second term, which will dominate at short periods, describes the consequences of excitation by differential ground motion and by large initial ground velocity. It is proportional to the natural frequency of the oscillator, peak horizontal ground velocity, and the transit time of the waves

along the length of the structure. The third term dominates the PSV spectral amplitudes at long periods and is proportional to the largest rocking angle of strong ground motion.

As the recording station moves away from the fault and the near-field terms in the ground motion diminish with distance, the spectral shapes of the motions at the fault, which are dominated by large initial peak ground velocities, will gradually and monotonically tend toward the amplitudes of spectra that are described by the familiar empirical scaling equations based on the recorded strong motion.

Data and Resources

No data were used in this article. Parts of some of the plots used in this article came from published sources listed in the references.

References

Applied Technology Council (ATC) (1996). *Seismic Evaluation and Retrofit of Concrete Buildings*, ATC Report No. ATC-40.

Aydinoglu, A. (2007). A response spectrum-based nonlinear assessment tool for practice: incremental response spectrum analysis (IRSA), *Indian Soc. Earthq. Technol. J.* **44,** no. 1, 169–192 (Paper 481).

Biot, M. A. (1934). Theory of vibration of buildings during earthquakes, *Z. Angew. Mat. Mech.* **14,** no. 4, 213–223.

Biot, M. A. (1941). A mechanical analyzer for the prediction of earthquake stresses, *Bull. Seismol. Soc. Am.* **31,** no. 2, 151–171.

Douglas, J. (2003). Earthquake ground motion estimation using strong-motion records: a review of equations for the estimation of peak ground acceleration and the response spectral ordinates, *Earth Sci. Rev.* **61,** no. 1–2, 43–104.

Federal Emergency Management Agency (FEMA) (1997). National Earthquake Hazards Reduction Program (NEHRP) guidelines for the seismic rehabilitation of buildings, FEMA Report No. FEMA-273 (Guidelines) and No. FEMA-274 (Commentary).

Federal Emergency Management Agency (FEMA) (2000). Prestandard and commentary for seismic rehabilitation of buildings, FEMA Report No. FEMA-356.

Freeman, S. (2007). Response spectra as a useful design and analysis tool for practicing structural engineers, *Indian Soc. Earthq. Technol. J.* **44,** no. 1, 25–37.

Goodman, L. E., E. Rosenblueth, and N. M. Newmark (1958). Aseismic design of firmly founded elastic structures, *Trans. ASCE* **120,** 782–802.

Gupta, I. D. (2007). Probabilistic seismic hazard analysis method for mapping of various parameters to estimate the earthquake effects on manmade structures, *Indian Soc. Earthq. Technol. J.* **44,** no. 1, 127–167.

Gupta, V. K., and M. D. Trifunac (1989). Investigation of building response to translational and rotational earthquake excitations, University of Southern California Department of Civil Engineering Report No. CE 89-02, available at http://www.usc.edu/dept/civil_eng/Earthquake_eng/.

Haskell, N. A. (1969). Elastic displacements in the near field of a propagating fault, *Bull. Seismol. Soc. Am.* **59,** 865–908.

Housner, G. W., and M. D. Trifunac (1967). Analysis of accelerograms—Parkfield earthquake, *Bull. Seismol. Soc. Am.* **57,** no. 6, 1193–1220.

Hudson, D. E. (1976). Strong motion earthquake accelerograms, Index Volume, Earthquake Engineering Research Laboratory 76-02, California Institute of Technology, Pasadena, California.

Jalali, R. S., and M. D. Trifunac (2007). Strength-reduction factors for structures subjected to differential near-source ground motion, *Indian Soc. Earthq. Technol. J.* **44,** no. 1, 285–304.

Jalali, R. S., and M. D. Trifunac (2008). A note on strength reduction factors for design of structures near earthquake faults, *Soil Dyn. Earthq. Eng.* **28,** no. 3, 212–222.

Jalali, R. S., M. D. Trifunac, G. Ghodrati Amiri, and M. Zahedi (2007). Wave-passage effects on strength-reduction factors for design of structures near earthquake faults, *Soil Dyn. Earthq. Eng.* **27,** no. 8, 703–711.

Lee, V. W. (2002). Empirical scaling of strong earthquake ground motion—part I: attenuation and scaling of response spectra, *Indian Soc. Earthq. Technol. J.*, **39,** no. 4, 219–254.

Lee, V. W. (2007). Empirical scaling and regression methods for earthquake strong-motion response spectra—a review, *Indian Soc. Earthq. Technol. J.* **44,** no. 1, 39–69.

Lee, V. W., and M. D. Trifunac (1987). Rocking strong earthquake acceleration, *Soil Dyn. Earthq. Eng.* **6,** no. 2, 75–89.

Mavroeidis, G. P., and A. S. Papageorgiou (2003). A mathematical representation of near-fault ground motions *Bull. Seismol. Soc. Am.* **93,** no. 3, 1099–1131.

Priestley, M. J. N., G. M. Calvi, and M. J. Kowalsky (2007). *Displacement-Based Seismic Design of Structures*, IUSS Press, Pavia, Italy.

Riddell, R., and N. M. Newmark (1979). Statistical analysis of the response of nonlinear systems subjected to earthquakes, in *Civil Engineering Studies*, Structural Research Series No. 468, University of Illinois, Urbana.

Takeo, M., and H. I. Ito (1997). What can be learned from rotational motions excited by earthquakes?, *Geophys. J. Int.* **129,** 319–329.

Todorovska, M. I., and M. D. Trifunac (1990). A note on excitation of long structures by ground waves, *J. Eng. Mech. Div. ASCE* **116,** no. 4, 952–964.

Trifunac, M. D. (1971). A method for synthesizing realistic strong ground motion, *Bull. Seismol. Soc. Am.* **61,** no. 6, 1739–1753.

Trifunac, M. D. (1974). A three-dimensional dislocation model for the San Fernando, California, earthquake of February 9, 1971, *Bull. Seismol. Soc. Am.* **64,** no. 1, 149–172.

Trifunac, M. D. (1978). Response spectra of earthquake ground motion, *ASCE*, **104,** EM5, 1081–1087.

Trifunac, M. D. (1982). A note on rotational components of earthquake motions on ground surface for incident body waves, *Soil Dyn. Earthq. Eng.* **1,** no. 1, 11–19.

Trifunac, M. D. (1993a). Broad-band extension of Fourier amplitude spectra of strong-motion acceleration, University of Southern California Department of Civil Engineering Report No. CE 93-01, available at http://www.usc.edu/dept/civil_eng/Earthquake_eng/.

Trifunac, M. D. (1993b). Long period Fourier amplitude spectra of strong motion acceleration, *Soil Dyn. Earthq. Eng.* **12,** no. 6, 363–382.

Trifunac, M. D. (1994). *Q* and high frequency strong motion spectra, *Soil Dyn. Earthq. Eng.* **13,** no. 3, 149–161.

Trifunac, M. D. (1998). Stresses and intermediate frequencies of strong motion acceleration, *Geofizika* **14,** 1–27.

Trifunac, M. D. (2003). 70th anniversary of Biot spectrum, in the *23rd Annual Indian Society of Earthquake Technology (ISET) Lecture*, Vol. **40**, no. 1, 19–50.

Trifunac, M. D. (2006). Effects of torsional and rocking excitations on the response of structures, in *Earthquake Source Asymmetry, Structural Media and Rotation Effects*, R. Teisseyre, M. Takeo, and E. Majewski (Editors), Springer, New York.

Trifunac, M. D. (2007). Early history of the response spectrum method, University of Southern California Department of Civil Engineering Report No. CE 07-01, available at http://www.usc.edu/dept/civil_eng/Earthquake_eng/.

Trifunac, M. D. (2009). The role of strong motion rotations in the response of structures near earthquake faults, *Soil Dyn. Earthq. Eng.* **29,** no. 2, 382–393.

Trifunac, M. D., and V. Gičev (2006). Response spectra for differential motion of columns, paper II: out-of-plane response, *Soil Dyn. Earthq. Eng.* **26,** no. 12, 1149–1160.

Trifunac, M. D., and M. I. Todorovska (1997). Response spectra and differential motion of columns, *Earthq. Eng. Struct. Dyn.* **26,** no. 2, 251–268.

Trifunac, M. D., and M. I. Todorovska (2001). A note on the usable dynamic range of accelerographs recording translation, *Soil Dyn. Earthq. Eng.*. **21,** no. 4, 275–286.

Trifunac, M. D., and F. E. Udwadia (1974). Parkfield, California, earthquake of June 27, 1966: a three-dimensional moving dislocation, *Bull. Seismol. Soc. Am.* **64,** no. 3, 511–533.

Udwadia, F. E., and M. D. Trifunac (1974). Characterization of response spectra through the statistics of oscillator response, *Bull. Seismol. Soc. Am.* **64,** no. 1, 205–219.

Veletsos, A. S., and N. M. Newmark (1960). Effect of inelastic behavior on the response of simple systems to earthquake motions, in the *Proceedings of the 2nd World Conference on Earthquake Engineering*, Vol. II, 859–912.

Veletsos, A. S., N. M. Newmark, and C. V. Celapati (1965). Deformation spectra for elastic and elastoplastic systems subjected to ground shock and earthquake motion, *Proceedings of the 3rd World Conference on Earthquake Engineering*, Vol. II, Wellington, New Zealand, 663–682.

Wong, H. L., and M. D. Trifunac (1979). Generation of artificial strong motion accelerograms, *Int. J. Earthq. Eng. Struct. Dyn.* **7,** no. 6, 509–527.

Zembaty, Z. (2007). Spatial seismic excitation and response spectra, *Indian Soc. Earthq. Technol. J.* **44,** no. 1, 233–258.

Department of Civil Engineering
Faculty of Engineering
University of Guilan
P.O. Box 3756
Rasht, Iran
saleh@guilan.ac.ir
(R.S.J.)

Department of Civil Engineering
University of Southern California
Los Angeles, California 90089
trifunac@usc.edu
(M.D.T.)

Manuscript received 15 May 2008